https://doi.org/10.5194/hess-2024-166
Preprint. Discussion started: 4 June 2024

Hydrology and Earth System Sciences Discussions
Open Access

Evaluating future hydrological changes in China under climate change

Danyang Gao[1, *], Albert S. Chen[1], Toby Richard Marthews[2], and Fayyaz Ali Memon[1]

[1] Centre for Water Systems, University of Exeter, Exeter, EX4 4QF, UK

[2] UK Centre for Ecology & Hydrology (UKCEH), Wallingford OX10 8BB, UK

[*] Corresponding Author

Corresponding author email: dg442@exeter.ac.uk

https://doi.org/10.5194/hess-2024-166
Preprint. Discussion started: 4 June 2024

Hydrology and Earth System Sciences
Discussions

Abstract

Projecting and understanding future hydrological changes in China are critical for effective water resource management and adaptation planning in response to climate variability. However, few studies have investigated runoff variability and flood and drought risks under climate change scenarios for the entire region of China at high resolution. In this study, we use the Joint UK Land Environment Simulator (JULES), specifically tailored for simulating hydrological processes in China at a 0.25-degree resolution. Downscaled and bias-corrected forcing data from Global Climate Models (GCMs), using the bias-correction and spatial disaggregation (BCSD) method, were used to drive the JULES model to project future hydrological processes under medium (SSP245) and high (SSP585) emission scenarios. The results indicate that annual runoff in China is projected to increase significantly under the high emission scenario, notably in the eastern and southern basins. Wetter summers and drier winters are expected in the south, while the opposite trend is expected in the north. Wetter conditions in the near future and drier summers in the far future are expected in northern China. Shifts from drier to wetter conditions are projected in the southeast and southwest areas, while the middle Yangtze River basin may experience the opposite trend. The flood risk is expected to increase in spring, summer, and autumn, along with heightened drought risk in winter, summer, and autumn. Southern China would face greater flood risk, while the central Yangtze River basin would face intensified drought risk, especially in the far future. These findings underscore the influence of different emission scenarios on flood and drought risks, emphasizing the need for proactive measures to enhance climate adaptation in the future.

Keywords: Hydrological simulation; Extreme hydrological risk; Land surface model; Climate change; CMIP6

https://doi.org/10.5194/hess-2024-166
Preprint. Discussion started: 4 June 2024

Hydrology and Earth System Sciences
Discussions

1 Introduction

Ongoing global warming is now having significant impacts on the hydrological cycle of many global ecosystems (Yin et al., 2018; Zhang et al., 2018; IPCC, 2023). Changes in the timing, magnitude, and seasonality of runoff may cause drought and flooding, posing threats to water security, which will lead to negative impacts on ecology, society and economy (Schewe et al., 2014; Miller et al., 2021). Therefore, the analysis of runoff responses to climate change is essential for investigating water security and extreme disaster events. Particularly in China, one of the most water-stressed nations (Zhai et al., 2022) with significant difference in regional precipitation (Jin et al., 2021), investigating the climate change impacts on runoff is essential for national and regional planning and the sustainable development of water resources.

Many scholars used different methods (e.g., hydrological models and the climatic elasticity methods) to study runoff under climate change in different regions of China. Zhao et al. (2019) developed an extended Variable Infiltration Capacity (VIC) macroscale hydrological model (named VIC-CAS) to project future changes in runoff components on the Tibetan Plateau based on Global Climate Models (GCMs) from the Coupled Model Inter-comparison Project Phase 5 (CMIP5). Gu et al. (2020) employed four lumped conceptual hydrological models to simulate runoff based on 31 GCMs from CMIP5 in 151 catchments in China. Guan et al. (2021) simulated the runoff conditions during the rest of 21 century based on Budyko framework and GCMs from the Coupled Model Inter-comparison Project Phase 6 (CMIP6) in 10 major river zones in China. Jin et al. (2021) assessed future water resource changes of the source region of the Yangtze River by the Soil and Water Assessment Tool (SWAT) and meteorological data of GCMs integrated by deep learning. Zhou et al. (2023a) analysed annual total runoff in 11 major basins in China by VIC. However, the model simulations in these studies were at the catchment scale that did not cover the whole region of China, while there are 2,221 rivers with catchment areas exceeding 1000 km^2 in China (Ministry of Water Resources,

https://doi.org/10.5194/hess-2024-166
Preprint. Discussion started: 4 June 2024

Hydrology and Earth System Sciences
Discussions

P. R. China and National Bureau of Statistics, P. R. China, 2013). Considering the numerous river basins (Fig. 1), the difficulty of obtaining hydrologic data in China (Lin et al., 2023) and the rare observation sites in some regions (e.g., high mountains), it is extremely difficult to calibrate and validate models for all catchments in China.

Some global studies related to future runoff under climate change covered China region (Cook et al., 2020; Chai et al., 2021; Hou et al., 2022; Wang et al., 2022; Miao et al., 2023). However, their analysis mainly based on results from CMIP5, CMIP6, Inter-Sectoral Impact Model Inter-Comparison Project (ISMIP2a) and Global Land Data Assimilation System (GLDAS), the resolutions of their runoff projections were coarse. Besides, the results were discussed mainly on the continental scale, the specific environment attributes of China were not particularly addressed. In this study, we will consider the features in the application the Joint UK Land Environment Simulator (JULES) to simulate hydrological processes with high resolution (0.25°) at the national scale.

The JULES model was developed by the UK Met Office evolved from the Met Office Surface Exchange Scheme (MOSES, Cox et al., 1999), which was the land surface scheme of UK Met Office Earth System Model, now used as a standalone land surface model to simulate the carbon fluxes (Clark et al., 2011), water, energy, and momentum (Best et al., 2011) between the land surface and the atmosphere. The model has been increasingly used for hydrological assessment (Zulkafli et al., 2013; Le Vine et al., 2016; Martínezde la Torre et al., 2019; Yang et al., 2019; Chou et al., 2022). However, the JULES model is rarely used in China, especially for hydrological simulation. Its ability to simulate hydrological process in China has yet to be examined.

In this study, we ask the following questions: (1) How well can the JULES model simulate hydrological processes in China at 0.25◦ resolution? (2) What will be the future runoff magnitude, year-to-year (inter-

https://doi.org/10.5194/hess-2024-166
Preprint. Discussion started: 4 June 2024

annual) variability and distribution in China? (3) whether and where will China face extreme runoff hazards risks (drought and flooding) under climate change? Addressing these questions will be crucial in enhancing our understanding of hydrological dynamics in China and in formulating effective adaptation and mitigation strategies to mitigate the impacts of changing climate conditions on water resources management and disaster risk reduction.

2 Methods

2.2 Historical Simulation using the JULES Model

Input for the JULES model includes meteorological forcing data and ancillary data. In its standard configuration, JULES recognises nine land cover types: broadleaf trees, needleleaf trees, C_3 (temperate) grass, C_4 (tropical) grass, shrubs, urban, inland water, bare soil and ice (Best et al., 2011). In this study, historical meteorological forcing data include near surface temperature, precipitation, downward shortwave and longwave radiation, wind speed, specific humidity and surface pressure are from the European Centre for Medium-Range Weather Forecasts Reanalysis 5 (ERA5, Hersbach et al., 2020). The ancillary data are from Marthews et al. (2022), considering nine land cover and seven soil layers.

To generate a reasonable initial condition, the JULES model was spun up in December of 1959 with 200 spin up cycles. Main run was during 1960 to 2014 covering all of China, using 0.25° resolution and a daily timestep. Observed discharge from the Global Runoff Data Centre (GRDC) was used to do monthly calibration and validation (Fig. 1). The model calibration was from 1962 to 1977, 1978 to 1986 were used for validation. The Pearson correlation coefficient (r) and Nash–Sutcliffe efficiency coefficient (NSE, Nash and Sutcliffe, 1970) were used to evaluate the model performance. The equations of r and NSE are shown in Eq. 1 and 2. Typically, an NSE greater than 0.5 indicates good alignment. Detailed standard thresholds

https://doi.org/10.5194/hess-2024-166
Preprint. Discussion started: 4 June 2024

Hydrology and Earth System Sciences
Discussions
Open Access

for NSE are provided in Marthews et al. (2022).

Figure 1. Location of GRDC stations for calibration and validation.

$$r = \frac{n\sum Q_o Q_m - (\sum Q_o)(\sum Q_m)}{\sqrt{[n\sum(Q_o)^2 - (\sum Q_o)^2][n\sum(Q_m)^2 - (\sum Q_m)^2]}} \quad (1)$$

$$\mathrm{NSE} = 1 - \frac{\sum_{t=1}^{T}(Q_o^t - Q_m^t)^2}{\sum_{t=1}^{T}(Q_o^t - \bar{Q}_o)^2} \quad (2)$$

where Q_m is modelled discharge, Q_o is observed discharge, $\bar{Q}_o$ is the mean of observed discharges, t is time, and n is the number of observations available for analysis.

2.2 Bias-Correction Spatial Disaggregation (BCSD) method

Future meteorological driving data are from GCMs in CMIP6. It was downscaled to 0.25° resolution based on ERA5 by bias-correction and spatial disaggregation (BCSD) method (Wood et al., 2004; Thrasher et al., 2022). This method compares the original GCMs output with climate observations during a common historical reference period, and uses the information obtained from the comparison to adjust future

https://doi.org/10.5194/hess-2024-166
Preprint. Discussion started: 4 June 2024

projections of GCMs, aiming to align the GCMs more closely with historical observation data and enhance their realism within the specific spatial area (Thrasher et al., 2022).

The BCSD method consists of three steps: preprocessing, bias correction, and spatial disaggregation. Preprocessing is only for the temperature variable; the main purpose is to detrend temperature so that their climate trends would not be affected by the bias correction. The 9-year moving average is calculated in each month individually. These trends are preserved and then re-incorporated into the adjusted data following the bias correction process. The bias correction process corrects the bias in GCMs output by observations, firstly, ERA5 datasets were interpolated to match the resolution of the selected GCMs. The data within ±15-day window from GCMs and ERA5 in a reference period from 1959 to 2014 were chosen to generate two cumulative distribution functions (CDFs). The quantile corresponding to each original GCM value was derived from the GCM-based CDF distribution for that particular day. Subsequently, this quantile was used to calculate the corresponding value from the ERA5-based CDF distribution. The final value is the bias-corrected GCMs data. Spatial disaggregation process interpolates the bias-corrected GCMs data to the observational resolution (0.25°). A smoothed daily climatology was generated over the reference period based on ERA5 by a Fast Fourier Transform retaining three harmonics. This climatology was then interpolated to the original grid of the GCMs and factored out of the bias-corrected GCMs either by subtracting from the temperature variables or by dividing from the other variables. The residual fields were bilinearly interpolated to the original 0.25° grid of the ERA5. Subsequently, the 0.25° climatology was factored back in either through addition to the temperature variables or multiplication by the other variables, yielding the final downscaled GCMs data.

We selected six GCMs from CMIP6 (EC-Earth3, INM-CM5-0, MIROC6, MPI-ESM1-2-HR, MRI-ESM2-0 and NorESM2-LM, shown in Table 1) that perform well for precipitation and temperature in China

https://doi.org/10.5194/hess-2024-166
Preprint. Discussion started: 4 June 2024

(Yang et al.,2021; Lu et al., 2022; Jia et al., 2023). First, we downscaled the precipitation of these six GCMs. By comparing the temporal root-mean-square error (RMSE) of annual precipitation in reference period over China, spatial Pearson correlation coefficient (*r*) and RMSE for multi-year average (1959–2014) daily precipitation, the three best performing GCMs were selected. Then we downscaled the near surface temperature, precipitation, downward shortwave and longwave radiation, wind speed, specific humidity and surface pressure of these three GCMs in middle and high emission scenarios (SSP245 and SSP585) as future input forcing data for JULES model.

Table 1. List of six CMIP6 GCMs and their reporting institutions and countries, and horizontal resolutions

GCM name	Modelling centre/Nation	Horizontal resolution in the standard configuration
EC-Earth3	EC-Earth consortium / Europe	0.703° × 0.703°
INM-CM5-0	Institute for Numerical Mathematics, Russian Academy of Science / Russia	1.5° × 2°
MIROC6	Atmosphere and Ocean Research Institute, Centre for Climate System Research - National Institute for Environmental Studies and Atmosphere and Ocean Research Institute / Japan	1.4° × 1.4°
MPI-ESM1-2-HR	Max Planck Institute for Meteorology /Germany	0.9375° × 0.9375°
MRI-ESM2-0	Meteorological Research Institute / Japan	1.125° × 1.125°
NorESM2-LM	Norwegian Climate Centre / Norway	1.875° × 1.875°

2.3 Future Projection under Climate Change

The downscaled GCMs for both the historical and future periods under the two scenarios were input into the calibrated and validated JULES model to simulate the hydrological processes. The runoff rate output

https://doi.org/10.5194/hess-2024-166
Preprint. Discussion started: 4 June 2024

Hydrology and Earth System Sciences Discussions

by JULES is in units of kg·m^{-2}·s^{-1}. We estimated the runoff at different time steps, measured in mm of depth. The annual and seasonal variations in runoff over China and its watersheds were analysed using the Mann-Kendall test (Mann, 1945; Kendall, 1975) to assess changing trends. For multi-year average runoff variation, the historical and future multi-year annual cycles of runoff over China and individual watersheds were compared. Differences in historical and future multi-year monthly runoff depths under two scenarios were calculated.

To evaluate the changes in extreme runoff under climate change, we calculated the seasonal 90th and 10th percentiles for each year based on the daily values. Regional mean values for China and individual basins were calculated to assess the changing trends of extreme runoff. Additionally, multi-year 90th and 10th percentile runoff depths were calculated for the historical period (1975-2014), near future (2021-2060), and far future (2061-2100) for each grid.

3 Results

3.1 JULES Model Evaluation

The JULES model performance for hydrology was evaluated against observed discharge. The comparison of observations and simulations during monthly calibration and monthly validation are shown in Fig. 2 and Fig. 3 , respectively. The r and NSE values are above 0.83 and 0.64, respectively, for calibrations, and greater than 0.78 and 0.58, respectively, for validation, indicating that the simulation outcomes are acceptable.

Most stations with good performance are near large rivers, indicating that the model simulates better in large rivers. This is mainly because the resolution in this study is 0.25°, which is slightly crude for simulating discharge of small rivers. Overall, JULES performs well in hydrological modelling.

https://doi.org/10.5194/hess-2024-166
Preprint. Discussion started: 4 June 2024

Hydrology and Earth System Sciences
Open Access
Discussions

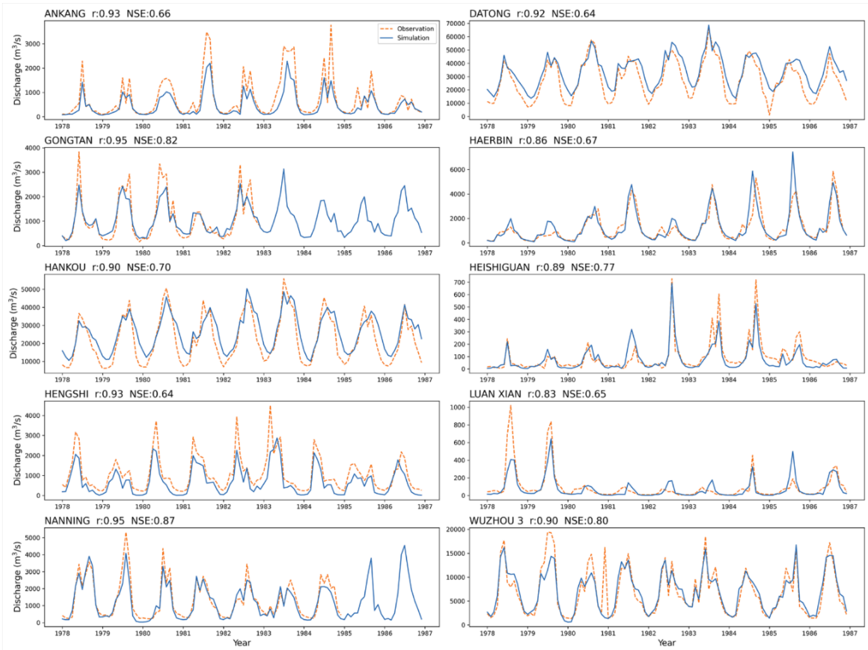

Figure 2. Comparison of observed and simulated discharge in monthly calibration

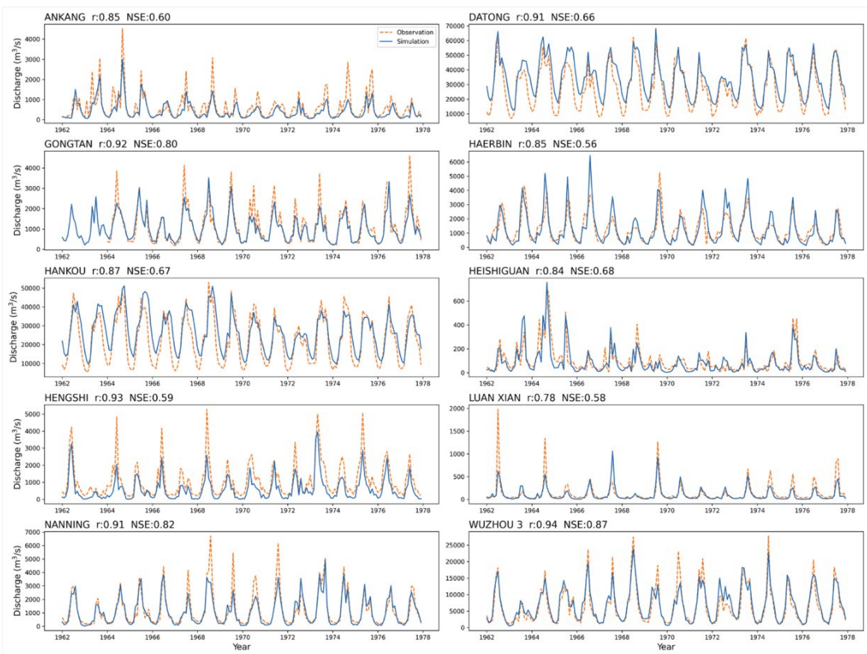

Figure 3. Comparison of observed and simulated discharge in monthly validation

https://doi.org/10.5194/hess-2024-166
Preprint. Discussion started: 4 June 2024

Hydrology and Earth System Sciences
Discussions
Open Access

3.2 Downscaled GCMs Evaluation

The annual precipitation from 1959 to 2014 over China of ERA5 and six downscaled GCMs is shown in Fig. 4, while r and RMSE between ERA5 and each downscaled GCMs are shown in Table 2. From the perspective of regional mean time series differences, the downscaled MPI-ESM1-2-HR performs the best. In terms of multi-year average precipitation, the downscaled EC-Earth3 simulates the best on the spatial pattern of precipitation (Table 2). Considering the combination of time series and spatial distribution, EC-Earth3, MPI-ESM1-2-HR and MRI-ESM2-0 are selected.

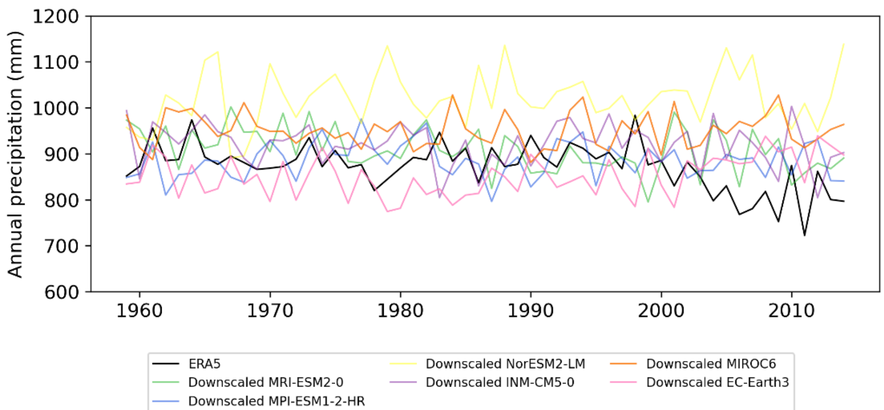

Figure 4. Comparison of annual precipitation between ERA5 and six downscaled GCMs

Table 2. r and RMSE for precipitation between ERA5 and six downscaled GCMs

GCMs	RMSE with time series	r of spatial distribution	RMSE of spatial distribution
MPI-ESM1-2-HR	67.057	0.954	0.819
EC-Earth3	74.059	0.964	0.691
MRI-ESM2-0	77.127	0.956	0.833
INM-CM5-0	78.289	0.944	0.928
MIROC6	104.562	0.941	1.075
NorESM2-LM	173.748	0.929	1.327

https://doi.org/10.5194/hess-2024-166
Preprint. Discussion started: 4 June 2024

Hydrology and Earth System Sciences
Discussions

Other annual meteorological variables from 1959 to 2014 over China for ERA5 and the three selected downscaled GCMs are shown in Fig. 5. The downscaled GCMs can simulate the trends of ERA5 for most variables. Among them, the simulation for surface temperature is the best. A slight difference in the trend modelling occurs in downward shortwave radiation, which is due to the original GCMs showing a clear decreasing trend in the historical period. For all downscaled GCMs and variables except precipitation, r of spatial distribution is greater 0.99. This indicates the selected GCMs can well reflect spatial pattern after downscaling.

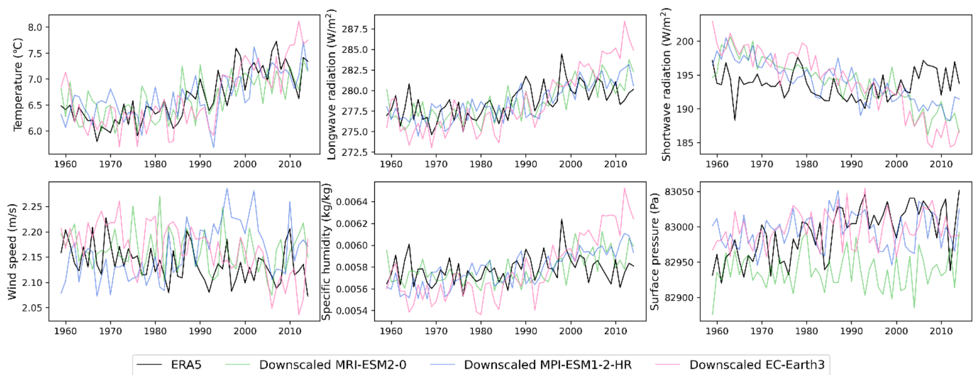

Figure 5. Comparison of annual meteorological variables between ERA5 and downscaled selected three GCMs

For each variable, to compare the bias before and after downscaling, the multi-year average values of original GCMs and downscaled GCMs are subtracted from the corresponding values of ERA5, respectively. The bias comparison map for every variable in ERA5 and the ensemble mean GCMs is shown in Fig. 6, while the bias between each GCM and ERA5 is shown in Fig. S1, S2 and S3. There are obvious differences between the original GCMs and ERA5, except for specific humidity and surface pressure. It can be clearly seen that after downscaling through the BCSD method, the bias between GCMs and ERA5 becomes smaller. Though the simulation for precipitation is less effective than for other variables (Fig. 6d), because precipitation is not continuous. Therefore, this set of BSCD GCMs data can be used for JULES models

https://doi.org/10.5194/hess-2024-166
Preprint. Discussion started: 4 June 2024

Hydrology and Earth System Sciences
Open Access
Discussions

established based on ERA5 to simulate hydrological process.

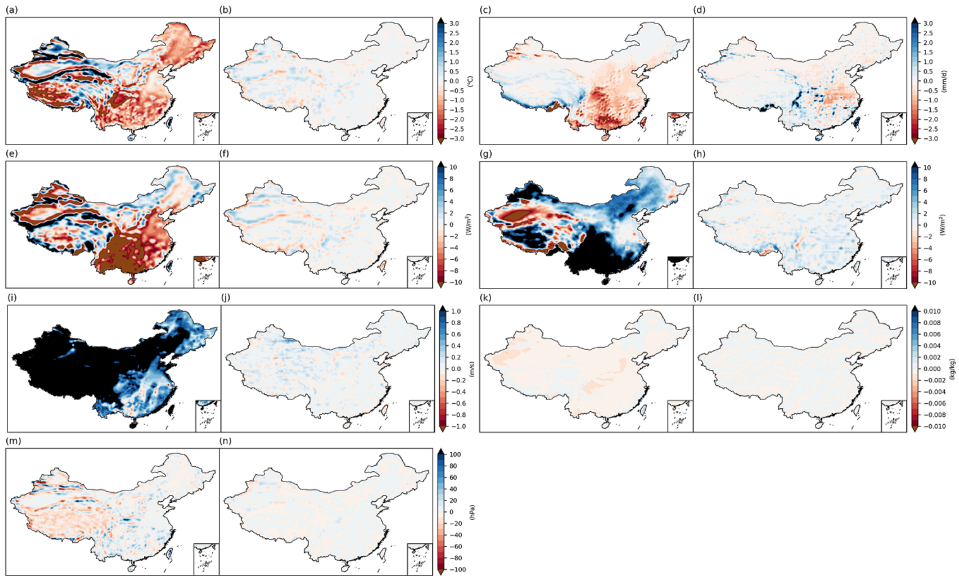

Figure 6. Bias comparison map for multi-year average daily surface temperature (a, b), precipitation (c, d), longwave radiation (e, f), shortwave radiation (g, h), wind speed (i, j), specific humidity (k, l) and surface pressure (m, n) between ERA5 and ensemble mean original GCMs (a, c, e, g, i, k, m), ERA5 and ensemble mean downscaled GCMs (b, d, f, h, j, l, n)

3.3 Runoff simulation results

3.3.1 Historical runoff simulation comparison

The historical runoff driven by three downscaled GCMs was simulated by the JULES model. The multi-year (1962-2000) average daily runoff depth simulated by ERA5 subtracted from the runoff simulated by downscaled GCMs is shown in Fig. 7. The seasonal differences are shown in Fig. 8. The difference of simulated runoff between the three GCMs and ERA5 are basically the same. In most areas of China, there is little difference between simulated runoff driven by GCMs and driven by ERA5. In the southeast region, there is an overestimation of the runoff simulated by GCMs. The overestimation in the east and the underestimation in south and middle area are more significant in summer. This is because bias of

https://doi.org/10.5194/hess-2024-166
Preprint. Discussion started: 4 June 2024

Hydrology and Earth System Sciences
Discussions
Open Access

precipitation in these areas are relatively large, especially in summer. For regional mean runoff over China, the difference between annual runoff based on ERA5 and GCMs is insignificant (Fig. 9a). The difference in summer varies a little more than the ones in the other three seasons (Fig. 10).

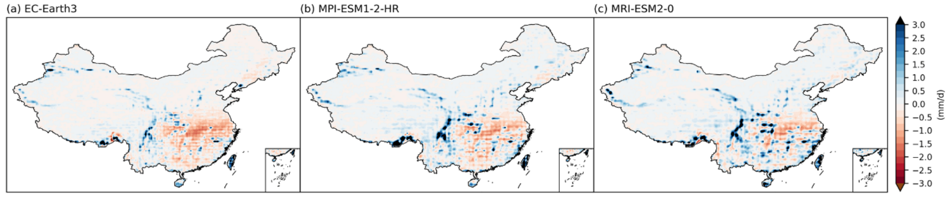

Figure 7. Multi-year (1962-2000) average daily runoff comparison map between JULES results based on ERA5 and (a) EC-Earth3, (b) MPI-ESM1-2-HR, (c) MRI-ESM2-0.

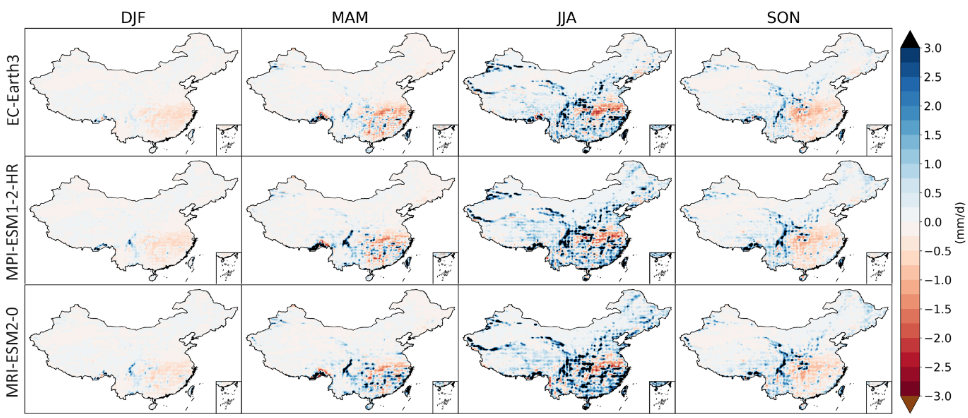

Figure 8. Multi-year (1962-2000) seasonal average daily runoff comparison map between JULES results based on ERA5 and three GCMs.

3.3.2 Runoff variation trends

The runoff variation over China from 1962 to 2100 is shown in Fig. 9a, and the variation trends were analysed using the Mann-Kendall test. The runoff is likely to increase significantly under the high emission scenario, while there is no obvious trend in the historical period under SSP245. Specifically, the runoff depth over China is projected to increase by 7.30 mm per decade between 2015 and 2100 under SSP585. This

https://doi.org/10.5194/hess-2024-166
Preprint. Discussion started: 4 June 2024

increase is primarily attributed to the rise in precipitation. Precipitation over China is expected to increase under both SSP245 and SSP585 scenarios (Fig. 9b). But the rising trend of runoff is not expected to be as pronounced as that of precipitation, because the increasing trend of evaporation is expected to be more significant in the future (Fig. 9c).

The annual runoff is likely to increase in eastern and southern China, including the Haihe River basin, Huaihe River basin, Pearl River basin, Songhua River basin, Southeast basin and Southwest basin under SSP585 (Fig. S4). Among these, the most dramatic increase is expected in the Southeast basin, with a trend rate of 41.45 mm per decade (while the increase trend rate of precipitation is 59.38 mm per decade). There are likely to be no significant trends in most basins under SSP245, with increasing trends only observed in partial eastern watersheds (Huaihe River basin and Songhua River basin) under SSP245.

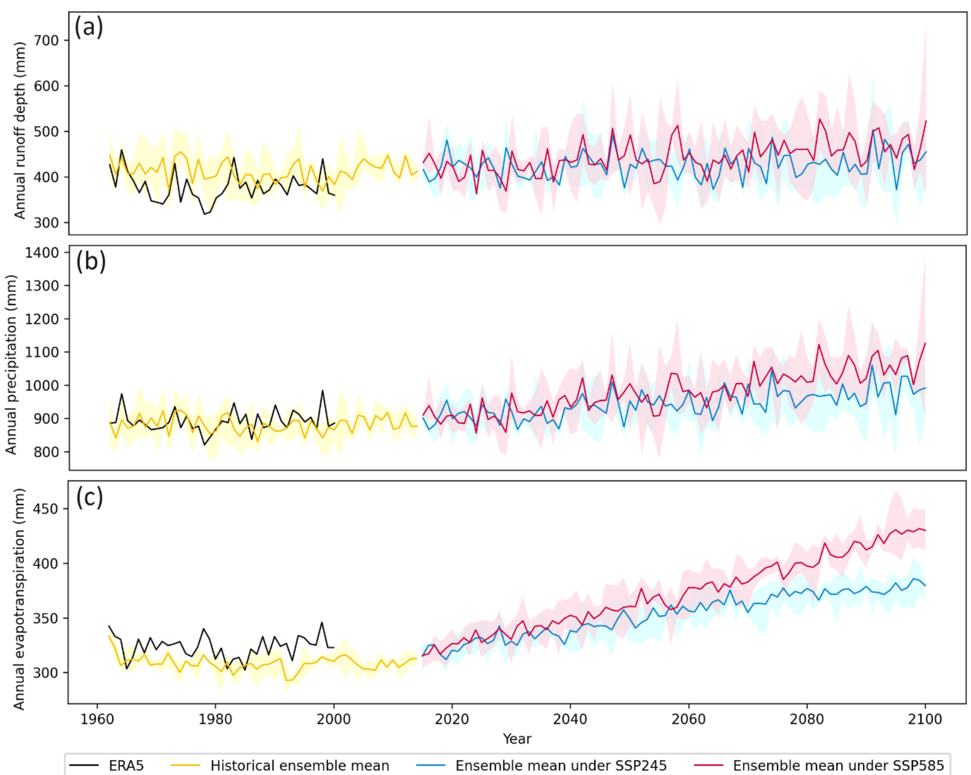

https://doi.org/10.5194/hess-2024-166
Preprint. Discussion started: 4 June 2024

Figure 9. Annual (a) runoff depth, (b) precipitation and (c) evapotranspiration over China. The black line represents the precipitation from ERA5, the simulated runoff and evapotranspiration based on ERA5. The yellow, blue and red lines are the ensemble mean precipitation from the three GCMs, simulated runoff and evapotranspiration driving by the three GCMs in historical, under SSP245 and SSP585, respectively. The shaded areas indicate the range between the maximum and minimum values of precipitation, simulated runoff depth and evapotranspiration based on the three GCMs.

From the perspective of seasonal runoff (Fig. 10), runoff in spring shows increasing trends in the future under both scenarios, (Fig. 10b), with the runoff depth over China likely to increase by 1.54 and 1.62 mm per decade between 2015 and 2100. Additionally, future runoff is expected to increase in summer (Fig. 10c) and autumn (Fig. 10d) under SSP585, with trend rates of 4.60 and 0.97 mm per decade, respectively.

The increase in runoff in each watershed is likely to occur mainly in spring and summer (Fig. S5). However, in the Continental basin, runoff in summer is expected to decrease while winter runoff is expected to increase both under both SSP245 and SSP585. Meanwhile, winter runoff in the Pearl River basin, Southeast basin and Yangtze River basin is likely to show a decreasing trend under SSP585. This also indicates that the variation trend of summer and winter runoff is likely to be opposite, with trends also differing between the northern and southern regions of China. Southern China is expected to experience wetter summers and drier winters under the high emission scenario, while the opposite trend is expected in the north.

https://doi.org/10.5194/hess-2024-166
Preprint. Discussion started: 4 June 2024

Hydrology and Earth System Sciences
Open Access
Discussions

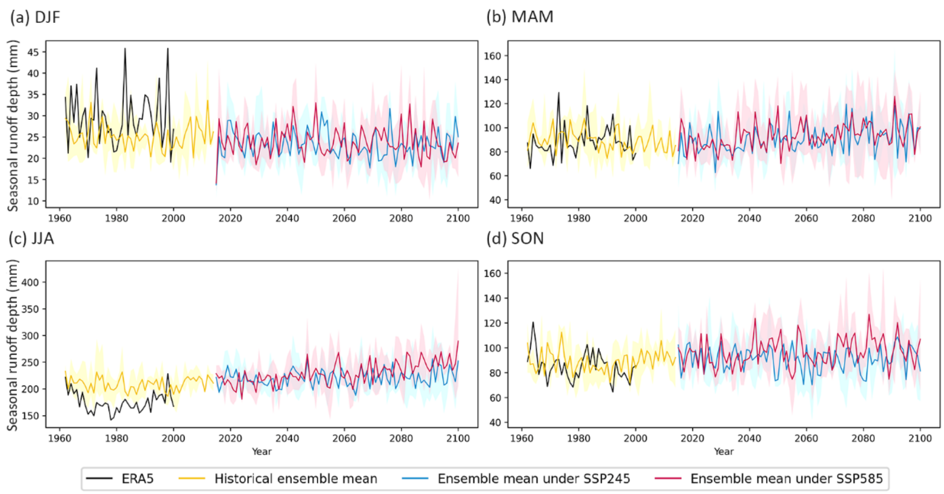

Figure 10. Seasonal runoff depth over China. The black line represents the simulated runoff based on ERA5. The yellow, blue and red line are the ensemble mean simulated runoff driving by three GCMs in historical, under SSP245 and SSP585, respectively. The shaded areas indicate the maximum and minimum ranges of simulated runoff depth based on three GCMs.

3.3.3 Multi-year average runoff variation

We divided future period into two parts: near future (2021-2060) and far future (2061-2100). The multi-year annual cycle of runoff in near, far future and historical period (1975-2014) was analysed (Fig. 11). Compared to historical period, more runoff is likely to occur in most months in the future, especially in summer. It is expected to increase most in far future under SSP585. Similar situation shows in most watersheds (Fig. S6). But the monthly runoff over Continental and Yellow River basin is greatest in near future under SSP585, while it is smaller in the far future under SSP585 than it in historical period in some summer months. This indicates wetter conditions in the near future and drier summers in the far future under SSP585 in the northern China.

https://doi.org/10.5194/hess-2024-166
Preprint. Discussion started: 4 June 2024

Hydrology and Earth System Sciences
Open Access
Discussions

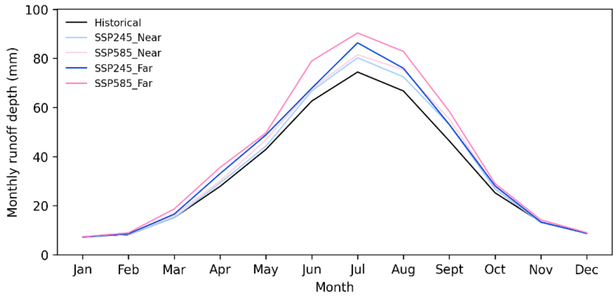

Figure 11. Multi-year annual cycle of runoff depth over China.

The multi-year monthly runoff changes in China are shown in Fig. 12. Under SSP245, the middle of the Yangtze River basin and the southern Liaohe River basin are likely to become drier (Fig. 12a) and then wetter (Fig. 12d). Similar trends are expected under SSP585 in the Southwest basin. Additionally, the multi-year monthly runoff is projected to significantly increase in southern China, including the Huaihe River, Pearl River, Southeast basins, and the eastern Yangtze River basin in the far future under SSP585 (Fig. 12e). The southeast and southwest areas are likely to become drier in the near future (Fig. 12c), followed by wetter conditions in the far future (Fig. 12f), while the middle Yangtze River basin is expected to experience the opposite trend.

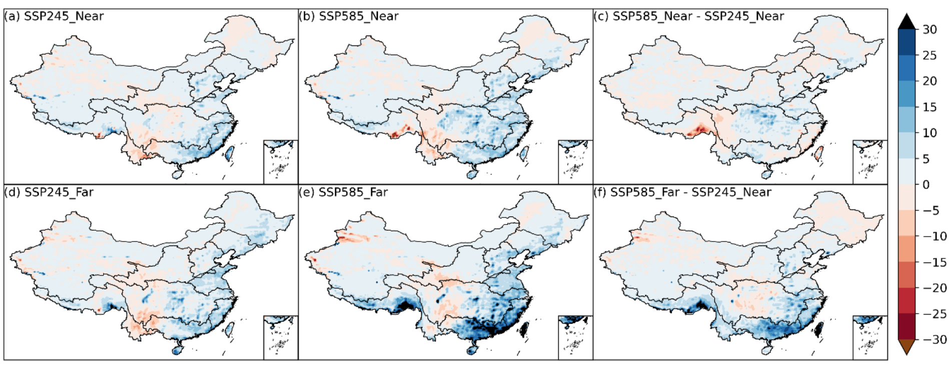

Figure 12. Multi-year monthly runoff changes in(a) 2021-2060 and (d) 2061-2100 under the SSP245, as well as (b) 2021-2060 and (e) 2061-2100 under the SSP585, relative to the historical period (1975-2014). (c) and (f) is the difference in multi-year ensemble mean monthly runoff depth between SSP245 and SSP585 in 2021-2060 and 2061-2100, respectively.

https://doi.org/10.5194/hess-2024-166
Preprint. Discussion started: 4 June 2024

Hydrology and Earth System Sciences
Discussions

3.3 Projected Extreme Runoff Change

The ensemble mean seasonal 90th and 10th percentile runoff depths over China for each year, based on daily values, are shown in Fig. 13. According to the Mann-Kendall test, the 90th percentile runoff is expected to increase in spring under both scenarios, as well as in summer and autumn under SSP585. Conversely, the 10th percentile runoff is expected to decrease in winter under SSP585, in summer under SSP245, and in autumn under both scenarios. These findings suggest an increased flooding risk in China during spring, summer, and autumn in the future, particularly under high emission scenarios, while the risk of drought is likely to increase in winter, summer, and autumn.

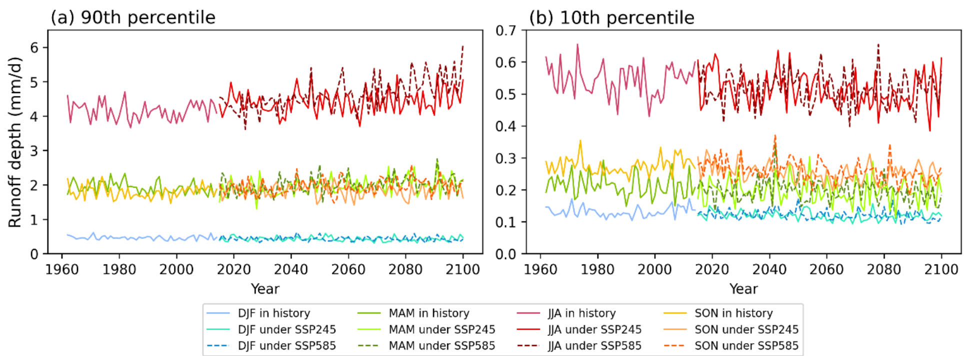

Figure 13. The ensemble mean seasonal (a) 90th and (b) 10th percentile runoff depth for each year during 1962 to 2100 over China.

Spatial changes of the multi-year 90th percentile runoff (Fig. 14) are similar to the changes in multi-year monthly runoff (Fig. 12). Compared to the historical period, future flood risks are likely to increase in southern China, particularly in the Southwest basin, Southeast basin, Pearl River basin, and southern Yangtze River basin, especially under SSP585 in the far future. In the near future, the Yangtze River basin is expected to face a higher flood risk under SSP585 compared to SSP245, while in the far future, the flood risk in southern China under SSP585 surpasses that under SSP245.

https://doi.org/10.5194/hess-2024-166
Preprint. Discussion started: 4 June 2024

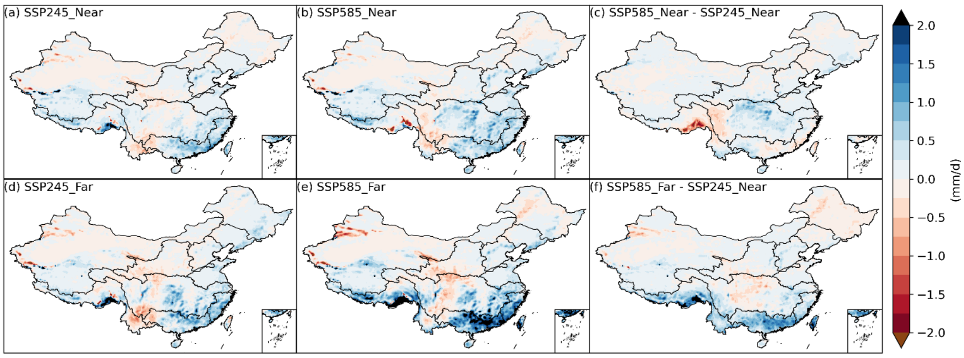

Figure 14. Multi-year ensemble mean 90th percentile runoff changes in (a) 2021-2060 and (d) 2061-2100 under the SSP245, as well as (b) 2021-2060 and (e) 2061-2100 under the SSP585, relative to the historical period (1975-2014). (c) and (f) is the difference in multi-year ensemble mean 90th percentile runoff depth between SSP245 and SSP585 in 2021-2060 and 2061-2100, respectively.

The multi-year changes in the 10th percentile runoff are illustrated in Fig. 15. In both SSP245 and SSP585 scenarios and in the near and the far futures, a decrease in the 10th percentile runoff is expected in central and southern China, with a more significant decline expected in the central Yangtze River basin, particularly under SSP585 in the far future (Fig. 15e). In the near future, only a small portion of the northeastern, southwestern, and southeastern regions are projected to experience a reduction in the 10th percentile runoff under SSP585 compared to SSP245, while in the far future, a decrease is also expected in the central Yangtze River basin. This suggests that under high emission scenarios, the central Yangtze River basin is likely to face a risk of drought.

https://doi.org/10.5194/hess-2024-166
Preprint. Discussion started: 4 June 2024

Hydrology and Earth System Sciences
Open Access
Discussions

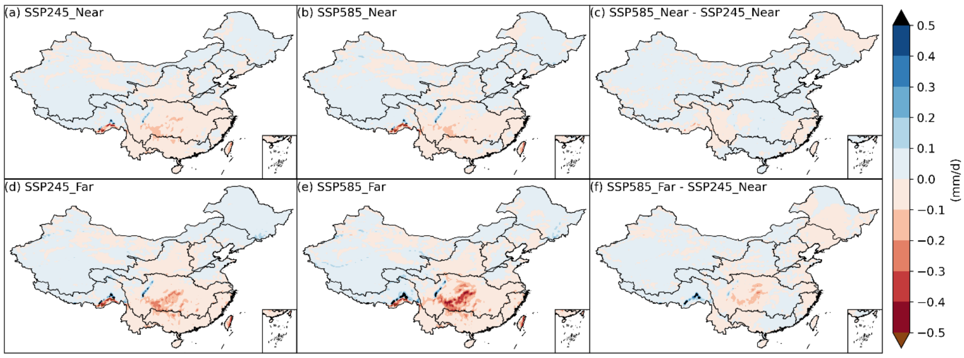

Figure 15. Multi-year ensemble mean 10th percentile runoff changes in (a) 2021-2060 and (d) 2061-2100 under the SSP245, as well as (b) 2021-2060 and (e) 2061-2100 under the SSP585, relative to the historical period (1975-2014). (c) and (f) is the difference in multi-year ensemble mean 10th percentile runoff depth between SSP245 and SSP585 in 2021-2060 and 2061-2100, respectively.

4 Discussion

4.1 Comparisons of runoff estimates in different studies

The change trends in annual runoff depth over China are similar to the results in Zhou et al. (2023a), indicating an overall wavelike rise, with the upward trend under SSP585 expected to be more severe than that under SSP245. However, the rise in runoff depth under SSP245 in this study does not pass the significance test in the Mann-Kendall trend test. In Guan et al. (2021), the increase in runoff in ten typical basins in China under SSP585 is not consistently greater than that under SSP245. This is attributed to Guan et al. (2021) using the climate elasticity method to project future runoff, which ignore complex hydrological and ecological processes.

The magnitude of simulated runoff depth in this study is larger than that in Zhou et al. (2023a). On one hand, it is mainly because the GCMs downscaled and historical hydrological modelling in this study are based on ERA5. ERA5 generally overestimates precipitation in the northern and western regions of China, even though it can capture seasonal variations and the broad spatial distributions in both magnitudes and

https://doi.org/10.5194/hess-2024-166
Preprint. Discussion started: 4 June 2024

Hydrology and Earth System Sciences
Open Access
Discussions

trends (Sun et al., 2021; Zhou et al., 2023c). On the other hand, the difference of simulated runoff depth may be caused by using different models and parameterization schemes.

The spatial variations of projected runoff in this study are similar to those in other studies (Cook et al.,2020; Wang et al., 2022; Zhou et al., 2023a). However, Cook et al. (2020) and Wang et al. (2022) analysed runoff change by percentage change, which cannot visually convey the actual changes in runoff volume. The percentage change in runoff is expected to be the largest in northern China, which could mislead readers into thinking that northern China is projected to face the most dramatic change in absolute runoff volume. However, the combined volume of runoff from six northern river basins, covering a total catchment area of 2.27 million km^2, contributes to less than 20% of the national total runoff. In contrast, four southern river basins, spanning a total catchment area of 2.86 million km^2, contribute to over 80% of the national total runoff (Zhang et al., 2011; Yang et al., 2022). Additionally, the runoff analysis in Cook et al. (2020) and Wang et al. (2022) were based on global coarse resolution and did not focus on the changes within China. Seasonal changes and changes in extreme runoff were not included in these studies (Cook et al.,2020; Wang et al., 2022; Zhou et al., 2023a).

4.2 Comparisons of extreme runoff in different studies

For extreme runoff, the drought risk in the central Yangtze River basin is projected to be the most severe and is expected to increase further in the far future compared to the near future, which aligns with the findings regarding projected hydrological drought changes in the severity reported (Gu et al., (2020). Regarding flooding, the relative change results of 100-year and 20-year flood quantiles in some GCMs indicated greater changes in eastern and southern China river basins (Gu et al., 2021), which are consistent with the results of this study. However, the drought and flooding analysis conducted by Gu et al. (2020, 2021) was performed under RCP8.5 in CMIP5, and focused on specific basins of China, rather than covering the entire country.

4.3 The dominant driving forces for runoff changes

Runoff changes in the future under climate change primarily stem from alterations in precipitation patterns, temperature variations, shifts in the hydrological cycle, and changes in the land surface. Continuous global warming is expected to increase the variability of water cycle, leading to more global monsoon precipitation, as well as the occurrence of very wet and very dry weather, climate events and seasons (IPCC, 2023). Specifically, in a warming climate, the water vapor holding capacity increases according to the Clausius-Clapeyron law (Clapeyron, 1834; Clausius, 1850). This results in more precipitable water and intensified precipitation extremes, which may cause flooding events. Warmer temperatures can enhance water evaporation from the ground. As soils desiccate, the overlying air may heat up further, intensifying evaporation and exacerbating drought conditions.

Precipitation patterns are influenced by the positions of tropical cyclones and extra-tropical cyclones shifting poleward, which could cause drought in some regions while leading to increasing flooding events in others (Zhang and Wang, 2017; Priestley and Catto, 2022).For perspective of the land surface, changes in vegetation response to rising CO_2 levels, coupled with modifications in vegetation cover and soil moisture in response to radiative climate change, are key contributors to projected increases in runoff (Zhou et al., 2023b).

4.4 Uncertainties of the study

Due to the difficulty in obtaining gauge discharge data in China (Lin et al., 2023), we utilized limited observational data to calibrate and validate the JULES model. Incorporating more site data distributed across various regions of China may improve the simulation performance of the model.

Additionally, this study did not consider the influence of hydraulic engineering on runoff, which could potentially alter the distribution of runoff and the occurrence of floods. Future research could involve integrating data on dams, reservoirs, and other hydraulic structures into hydrological models to assess their effects on runoff dynamics. This approach could investigate how human activities impact hydrological processes and contribute to flood vulnerability.

The land surface model and precipitation data products introduce uncertainties into runoff extremes. These uncertainties may increase during the propagation through models when projecting runoff extremes in southeast China, but decreased in north China (Marthews et al., 2020).

GCMs also introduce uncertainty into hydrological modelling, and the selection of GCMs can significantly affect the climate change impacts on hydrology (Her et al., 2019). Therefore, in this study, three GCMs that are deemed more suitable for China were selected based on their precipitation downscaling performance among the six GCMs evaluated. While using and screening more GCMs for hydrological simulation may help reduce uncertainty, it also necessitates substantial computing resources.

5 Conclusion

In this study, we constructed a JULES model configuration specifically tailored for simulating hydrological processes in China and employed the BCSD method to downscale and bias correct the three selected GCMs. Using the GCMs to drive the JULES model, the future hydrological processes under medium and high emission scenarios were projected. The main findings are summarized below:

(1) The JULES model performed well in simulating hydrological processes in China at 0.25° resolution. The BCSD method can effectively reduce the bias between GCMs and ERA5 in China. There are minimal differences between downscaled-GCM-driven and ERA5-driven runoff using the JULES model across most of China. An overestimation of runoff is shown in the southeast region, particularly pronounced during summer months.

(2) Runoff variations across China are projected to increase significantly under the high emission scenario, with the runoff depth increasing by 7.30 mm per decade from 2015 to 2100. Regional analysis suggests that eastern and southern basins, notably the Southeast basin, are expected to experience the most significant increases in runoff. Seasonal runoff trends indicate an overall increase, particularly in spring, summer, and autumn under the high emission scenario, with varying trends observed across different watersheds. Notably, variations in runoff trends between northern and southern China suggest contrasting seasonal patterns, with wetter summers and drier winters expected in the south under the high emission scenario, while the opposite trend is expected in the north.

(3) An increase in runoff across most months in the future, compared to the historical period, is particularly evident in summer and expected to intensify in the far future under SSP585. Wetter conditions in the near future and drier summers in the far future under SSP585 are expected in northern China. Additionally, changes in multi-year monthly runoff patterns reveal regional variations, with some basins projected to become drier and then wetter under SSP245, while significant increases are expected in southern China in the far future under SSP585. Moreover, shifts from drier to wetter conditions are expected in the southeast and southwest areas, while the middle Yangtze River basin may experience the opposite trend.

(4) Flood risk during spring, summer, and autumn may increase in the future, particularly under the high emission scenario, while the drought risk is likely to increase in winter, summer, and autumn. Spatial changes in the multi-year 90th percentile runoff indicate future flood risks are expected to rise in southern China, especially in the Southwest basin, Southeast basin, Pearl River basin, and southern Yangtze River basin, particularly under the high emission scenario in the far future. Conversely, decreases in the 10th percentile runoff suggest a heightened risk of drought in central and southern China, with the central Yangtze River basin facing significant declines, particularly under the high emission scenario in the far future. These

findings highlight the influence of different emission scenarios on flood and drought risks, it is important to take proactive measures to enhance climate adaptations in the future.

Acknowledgements

This work was supported by the China Scholarship Council. Danyang Gao received additional support through the visiting scientist program under the Hydro-JULES scheme at UK Centre for Ecology & Hydrology (UKCEH) in November 2022. We acknowledge the World Climate Research Programme, which, through its Working Group on Coupled Modelling, coordinated and promoted CMIP6. We thank the climate modelling groups for producing and making available their model output, the Earth System Grid Federation (ESGF) for archiving the data and providing access, and the multiple funding agencies who support CMIP6 and ESGF. We also acknowledge the use of ERA5 data produced by ECMWF. The running of JULES and analysis of results in this work were performed on the JASMIN super-data-cluster (Lawrence et al., 2012). JASMIN is managed and delivered by the UK Science and Technology Facilities Council (STFC) Centre for Environmental Data Archival (CEDA).

Data availability

The data and code that support the study are available from the corresponding author upon request.

Author contribution

DG: methodology, modelling, formal analysis, and writing - original draft. AC: supervision, methodology, and writing - review and editing. TM: supervision, modelling, and writing – review and editing. FM: supervision, methodology, and writing – review and editing.

Competing interests

The contact author has declared that none of the authors has any competing interests.

https://doi.org/10.5194/hess-2024-166
Preprint. Discussion started: 4 June 2024

References

Bian, G., Zhang, J., Chen, J., Song, M., He, R., Liu, C., Liu, Y., Bao, Z., Lin, Q., & Wang, G. (2021). Projecting Hydrological Responses to Climate Change Using CMIP6 Climate Scenarios for the Upper Huai River Basin, China. *Frontiers in Environmental Science*, *9*. https://www.frontiersin.org/articles/10.3389/fenvs.2021.759547

Calvin, K., Dasgupta, D., Krinner, G., Mukherji, A., Thorne, P. W., Trisos, C., Romero, J., Aldunce, P., Barrett, K., Blanco, G., Cheung, W. W. L., Connors, S., Denton, F., Diongue-Niang, A., Dodman, D., Garschagen, M., Geden, O., Hayward, B., Jones, C., … Péan, C. (2023). *IPCC, 2023: Climate Change 2023: Synthesis Report. Contribution of Working Groups I, II and III to the Sixth Assessment Report of the Intergovernmental Panel on Climate Change [Core Writing Team, H. Lee and J. Romero (eds.)]. IPCC, Geneva, Switzerland.* (First). Intergovernmental Panel on Climate Change (IPCC). https://doi.org/10.59327/IPCC/AR6-9789291691647

Chai, Y., Berghuijs, W. R., Naudts, K., Janssen, T. A. J., Yao, Y., & Dolman, H. (2021). Using precipitation sensitivity to temperature to adjust projected global runoff. *Environmental Research Letters*, *16*(12), 124032. https://doi.org/10.1088/1748-9326/ac3795

Chen, H., Sun, J., Lin, W., & Xu, H. (2020). Comparison of CMIP6 and CMIP5 models in simulating climate extremes. *Science Bulletin*, *65*. https://doi.org/10.1016/j.scib.2020.05.015

Chen, Y., Wang, L., Shi, X., Zeng, C., Wang, Y., Wang, G., Qiangba, C., Yue, C., Sun, Z., Renzeng, O., & Zhang, F. (2023). Impact of Climate Change on the Hydrological Regimes of the Midstream Section of the Yarlung Tsangpo River Basin Based on SWAT Model. *Water*, *15*(4), Article 4. https://doi.org/10.3390/w15040685

Chou, H.-K., Heuminski de Avila, A. M., & Bray, M. (2022). Evaluating the Atibaia River hydrology using

JULES6.1. *Geoscientific Model Development*, *15*(13), 5233–5240. https://doi.org/10.5194/gmd-15-5233-2022

Clapeyron, É. (1834). Mémoire sur la puissance motrice de la chaleur. *Journal de l'École Polytechnique*, *23*, 153190 (in French). https://gallica.bnf.fr/ark:/12148/bpt6k3414331n

Clausius, R. (1850). Ueber die bewegende Kraft der Wärme und die Gesetze, welche sich daraus für die Wärmelehre selbst ableiten lassen. *Annalen der Physik*, *155*(4), 500-524 (in German). https://doi.org/10.1002/andp.18501550403

Cook, B. I., Mankin, J. S., Marvel, K., Williams, A. P., Smerdon, J. E., & Anchukaitis, K. J. (2020). Twenty-First Century Drought Projections in the CMIP6 Forcing Scenarios. *Earth's Future*, *8*(6), e2019EF001461. https://doi.org/10.1029/2019EF001461

Eyring, V., Bony, S., Meehl, G. A., Senior, C. A., Stevens, B., Stouffer, R. J., & Taylor, K. E. (2016). Overview of the Coupled Model Intercomparison Project Phase 6 (CMIP6) experimental design and organization. *Geoscientific Model Development*, *9*(5), 1937–1958. https://doi.org/10.5194/gmd-9-1937-2016

Gu, L., Chen, J., Yin, J., Xu, C.-Y., & Zhou, J. (2020). Responses of Precipitation and Runoff to Climate Warming and Implications for Future Drought Changes in China. *Earth's Future*, *8*(10), e2020EF001718. https://doi.org/10.1029/2020EF001718

Gu, L., Yin, J., Zhang, H., Wang, H.-M., Yang, G., & Wu, X. (2021). On future flood magnitudes and estimation uncertainty across 151 catchments in mainland China. *International Journal of Climatology*, *41*(S1), E779–E800. https://doi.org/10.1002/joc.6725

Guan, X., Zhang, J., Bao, Z., Liu, C., Jin, J., & Wang, G. (2021). Past variations and future projection of runoff in typical basins in 10 water zones, China. *Science of The Total Environment*, *798*, 149277.

https://doi.org/10.5194/hess-2024-166
Preprint. Discussion started: 4 June 2024

https://doi.org/10.1016/j.scitotenv.2021.149277

Her, Y., Yoo, S.-H., Cho, J., Hwang, S., Jeong, J., & Seong, C. (2019). Uncertainty in hydrological analysis of climate change: Multi-parameter vs. multi-GCM ensemble predictions. *Scientific Reports*, *9*(1), 4974. https://doi.org/10.1038/s41598-019-41334-7

Hersbach, H., Bell, B., Berrisford, P., Hirahara, S., Horányi, A., Muñoz-Sabater, J., Nicolas, J., Peubey, C., Radu, R., Schepers, D., Simmons, A., Soci, C., Abdalla, S., Abellan, X., Balsamo, G., Bechtold, P., Biavati, G., Bidlot, J., Bonavita, M., … Thépaut, J. (2020). The ERA5 global reanalysis. *Quarterly Journal of the Royal Meteorological Society*, *146*(730), 1999–2049. https://doi.org/10.1002/qj.3803

Hou, Y., Guo, H., Yang, Y., & Liu, W. (2023). Global Evaluation of Runoff Simulation From Climate, Hydrological and Land Surface Models. *Water Resources Research*, *59*(1), e2021WR031817. https://doi.org/10.1029/2021WR031817

Jin, H., Chen, X., Wu, P., Song, C., & Xia, W. (2021). Evaluation of spatial-temporal distribution of precipitation in mainland China by statistic and clustering methods. *Atmospheric Research*, *262*, 105772. https://doi.org/10.1016/j.atmosres.2021.105772

Kendall, M. G. (1975). *Rank correlation methods* (4th ed., 2d impression). Griffin.

Lawrence, B. N., Bennett, V., Churchill, J., Juckes, M., Kershaw, P., Oliver, P., Pritchard, M., & Stephens, A. (2012). The JASMIN super-data-cluster (arXiv:1204.3553). arXiv. https://doi.org/10.48550/arXiv.1204.3553

Le Vine, N., Butler, A., McIntyre, N., & Jackson, C. (2016). Diagnosing hydrological limitations of a land surface model: Application of JULES to a deep-groundwater chalk basin. *Hydrology and Earth System Sciences*, *20*(1), 143–159. https://doi.org/10.5194/hess-20-143-2016

Lin, J., Bryan, B. A., Zhou, X., Lin, P., Do, H. X., Gao, L., Gu, X., Liu, Z., Wan, L., Tong, S., Huang, J.,

https://doi.org/10.5194/hess-2024-166
Preprint. Discussion started: 4 June 2024

Wang, Q., Zhang, Y., Gao, H., Yin, J., Chen, Z., Duan, W., Xie, Z., Cui, T., … Yang, Z. (2023). Making China’s water data accessible, usable and shareable. *Nature Water*, *1*(4), Article 4. https://doi.org/10.1038/s44221-023-00039-y

Lu, K., Arshad, M., Ma, X., Ullah, I., Wang, J., & Shao, W. (2022). Evaluating observed and future spatiotemporal changes in precipitation and temperature across China based on CMIP6-GCMs. *International Journal of Climatology*, *42*(15), 7703–7729. https://doi.org/10.1002/joc.7673

Mann, H. B. (1945). Nonparametric Tests Against Trend. *Econometrica*, *13*(3), 245–259. https://doi.org/10.2307/1907187

Marthews, T. R., Blyth, E. M., Martínez-de la Torre, A., & Veldkamp, T. I. E. (2020). A global-scale evaluation of extreme event uncertainty in the *eartH2Observe* project. *Hydrology and Earth System Sciences*, *24*(1), 75–92. https://doi.org/10.5194/hess-24-75-2020

Marthews, T. R., Dadson, S. J., Clark, D. B., Blyth, E. M., Hayman, G. D., Yamazaki, D., Becher, O. R. E., Martínez-de la Torre, A., Prigent, C., & Jiménez, C. (2022). Inundation prediction in tropical wetlands from JULES-CaMa-Flood global land surface simulations. *Hydrology and Earth System Sciences*, *26*(12), 3151–3175. https://doi.org/10.5194/hess-26-3151-2022

Martínez-de la Torre, A., Blyth, E. M., & Weedon, G. P. (2019). Using observed river flow data to improve the hydrological functioning of the JULES land surface model (vn4.3) used for regional coupled modelling in Great Britain (UKC2). *Geoscientific Model Development*, *12*(2), 765–784. https://doi.org/10.5194/gmd-12-765-2019

Miao, C., Wu, Y., Fan, X., & Su, J. (2023). Projections of Global Land Runoff Changes and Their Uncertainty Characteristics During the 21st Century. *Earth’s Future*, *11*(4), e2022EF003286. https://doi.org/10.1029/2022EF003286

https://doi.org/10.5194/hess-2024-166
Preprint. Discussion started: 4 June 2024

Miller, O. L., Miller, M. P., Longley, P. C., Alder, J. R., Bearup, L. A., Pruitt, T., Jones, D. K., Putman, A. L., Rumsey, C. A., & McKinney, T. (2021). How Will Baseflow Respond to Climate Change in the Upper Colorado River Basin? *Geophysical Research Letters*, *48*(22), e2021GL095085. https://doi.org/10.1029/2021GL095085

Nash, J. E., & Sutcliffe, J. V. (1970). River flow forecasting through conceptual models part I — A discussion of principles. *Journal of Hydrology*, *10*(3), 282–290. https://doi.org/10.1016/0022-1694(70)90255-6

O'Neill, B. C., Tebaldi, C., van Vuuren, D. P., Eyring, V., Friedlingstein, P., Hurtt, G., Knutti, R., Kriegler, E., Lamarque, J.-F., Lowe, J., Meehl, G. A., Moss, R., Riahi, K., & Sanderson, B. M. (2016). The Scenario Model Intercomparison Project (ScenarioMIP) for CMIP6. *Geoscientific Model Development*, *9*(9), 3461–3482. https://doi.org/10.5194/gmd-9-3461-2016

Priestley, M. D. K., & Catto, J. L. (2022). Future changes in the extratropical storm tracks and cyclone intensity, wind speed, and structure. *Weather and Climate Dynamics*, *3*(1), 337–360. https://doi.org/10.5194/wcd-3-337-2022

Riahi, K., van Vuuren, D. P., Kriegler, E., Edmonds, J., O'Neill, B. C., Fujimori, S., Bauer, N., Calvin, K., Dellink, R., Fricko, O., Lutz, W., Popp, A., Cuaresma, J. C., Kc, S., Leimbach, M., Jiang, L., Kram, T., Rao, S., Emmerling, J., … Tavoni, M. (2017). The Shared Socioeconomic Pathways and their energy, land use, and greenhouse gas emissions implications: An overview. *Global Environmental Change*, *42*, 153–168. https://doi.org/10.1016/j.gloenvcha.2016.05.009

Schewe, J., Heinke, J., Gerten, D., Haddeland, I., Arnell, N. W., Clark, D. B., Dankers, R., Eisner, S., Fekete, B. M., Colón-González, F. J., Gosling, S. N., Kim, H., Liu, X., Masaki, Y., Portmann, F. T., Satoh, Y., Stacke, T., Tang, Q., Wada, Y., … Kabat, P. (2014). Multimodel assessment of water scarcity under climate change. *Proceedings of the National Academy of Sciences*, *111*(9), 3245–3250.

https://doi.org/10.1073/pnas.1222460110

Sun, H., Su, F., Yao, T., He, Z., Tang, G., Huang, J., Zheng, B., Meng, F., Ou, T., & Chen, D. (2021). General overestimation of ERA5 precipitation in flow simulations for High Mountain Asia basins. *Environmental Research Communications*, *3*(12), 121003. https://doi.org/10.1088/2515-7620/ac40f0

Thrasher, B., Wang, W., Michaelis, A., Melton, F., Lee, T., & Nemani, R. (2022). NASA Global Daily Downscaled Projections, CMIP6. *Scientific Data*, *9*(1), Article 1. https://doi.org/10.1038/s41597-022-01393-4

Wang, A., Miao, Y., Kong, X., & Wu, H. (2022). Future Changes in Global Runoff and Runoff Coefficient From CMIP6 Multi-Model Simulation Under SSP1-2.6 and SSP5-8.5 Scenarios. *Earth's Future*, *10*(12), e2022EF002910. https://doi.org/10.1029/2022EF002910

Wen, K., Gao, B., & Li, M. (2021). Quantifying the Impact of Future Climate Change on Runoff in the Amur River Basin Using a Distributed Hydrological Model and CMIP6 GCM Projections. *Atmosphere*, *12*(12), Article 12. https://doi.org/10.3390/atmos12121560

Wood, A. W., Leung, L. R., Sridhar, V., & Lettenmaier, D. P. (2004). Hydrologic Implications of Dynamical and Statistical Approaches to Downscaling Climate Model Outputs. *Climatic Change*, *62*(1), 189–216. https://doi.org/10.1023/B:CLIM.0000013685.99609.9e

Yang, H., Huntingford, C., Wiltshire, A., Sitch, S., & Mercado, L. (2019). Compensatory climate effects link trends in global runoff to rising atmospheric CO2 concentration. *Environmental Research Letters*, *14*(12), 124075. https://doi.org/10.1088/1748-9326/ab5c6f

Yang, L., Zhao, G., Tian, P., Mu, X., Tian, X., Feng, J., & Bai, Y. (2022). Runoff changes in the major river basins of China and their responses to potential driving forces. *Journal of Hydrology*, *607*, 127536. https://doi.org/10.1016/j.jhydrol.2022.127536

Yang, X., Zhou, B., Xu, Y., & Han, Z. (2021). CMIP6 Evaluation and Projection of Temperature and Precipitation over China. *Advances in Atmospheric Sciences*, *38*(5), 817–830. https://doi.org/10.1007/s00376-021-0351-4

Yin, J., Gentine, P., Zhou, S., Sullivan, S. C., Wang, R., Zhang, Y., & Guo, S. (2018). Large increase in global storm runoff extremes driven by climate and anthropogenic changes. *Nature Communications*, *9*(1), Article 1. https://doi.org/10.1038/s41467-018-06765-2

Zhai, R., Tao, F., Chen, Y., Dai, H., Liu, Z., & Fu, B. (2022). Future water security in the major basins of China under the 1.5 °C and 2.0 °C global warming scenarios. *Science of The Total Environment*, *849*, 157928. https://doi.org/10.1016/j.scitotenv.2022.157928

Zhang, C., & Wang, Y. (2017). Projected Future Changes of Tropical Cyclone Activity over the Western North and South Pacific in a 20-km-Mesh Regional Climate Model. *Journal of Climate*, *30*(15), 5923–5941. https://doi.org/10.1175/JCLI-D-16-0597.1

Zhang, X., Tang, Q., Liu, X., Leng, G., & Di, C. (2018). Nonlinearity of Runoff Response to Global Mean Temperature Change Over Major Global River Basins. *Geophysical Research Letters*, *45*(12), 6109–6116. https://doi.org/10.1029/2018GL078646

Zhang, Z., Chen, X., Xu, C.-Y., Yuan, L., Yong, B., & Yan, S. (2011). Evaluating the non-stationary relationship between precipitation and streamflow in nine major basins of China during the past 50 years. *Journal of Hydrology*, *409*(1), 81–93. https://doi.org/10.1016/j.jhydrol.2011.07.041

Zhou, J., Lu, H., Yang, K., Jiang, R., Yang, Y., Wang, W., & Zhang, X. (2023a). Projection of China's future runoff based on the CMIP6 mid-high warming scenarios. *Science China Earth Sciences*, *66*(3), 528–546. https://doi.org/10.1007/s11430-022-1055-5

Zhou, S., Yu, B., Lintner, B. R., Findell, K. L., & Zhang, Y. (2023b). Projected increase in global runoff dominated by land surface changes. *Nature Climate Change*, *13*(5), 442–449. https://doi.org/10.1038/s41558-023-01659-8

Zhou, Z., Chen, S., Li, Z., & Luo, Y. (2023c). An Evaluation of CRA40 and ERA5 Precipitation Products over China. *Remote Sensing*, *15*(22), Article 22. https://doi.org/10.3390/rs15225300

Zulkafli, Z., Buytaert, W., Onof, C., Lavado, W., & Guyot, J. L. (2013). A critical assessment of the JULES land surface model hydrology for humid tropical environments. *Hydrology and Earth System Sciences*, *17*(3), 1113–1132. https://doi.org/10.5194/hess-17-1113-2013